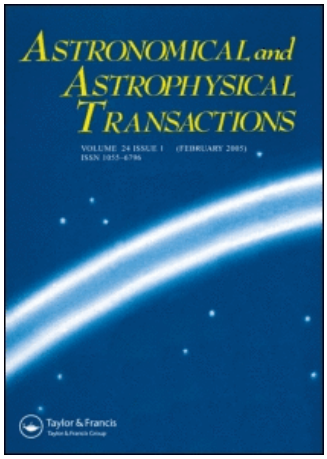

Astronomical & Astrophysical Transactions
The Journal of the Eurasian Astronomical Society
Publication details, including instructions for authors and subscription information:
http://www.informaworld.com/smpp/title~content=t713453505

Structure and variability of hot-star winds

Kholtygin; Brown; Cassinelli; Fabrika; Monin; Surkov

Online Publication Date: 01 January 2003
To cite this Article: Kholtygin, Brown, Cassinelli, Fabrika, Monin and Surkov (2003) 'Structure and variability of hot-star winds', Astronomical & Astrophysical Transactions, 22:4, 499 - 512
To link to this article: DOI: 10.1080/1055679031000139424
URL: http://dx.doi.org/10.1080/1055679031000139424

Astronomical and Astrophysical Transactions
Vol. 22, Nos. 4–5, August–October 2003, pp. 499–512

STRUCTURE AND VARIABILITY OF HOT-STAR WINDS

A. F. KHOLTYGIN[a,*], J. C. BROWN[b], J. P. CASSINELLI[c], S. N. FABRIKA[d], D. N. MONIN[d] and A. E. SURKOV[d]

[a]Astronomical Institute, St Petersburg University, St Petersburg, Universiteskij Prospect 28, 198504, Russia;
[b]Department of Physics and Astronomy, University of Glasgow, Glasgow G12 8QQ, UK;
[c]Department of Astronomy, University of Wisconsin, 475 N. Charter Street, Madison, Wisconsin 53711, USA;
[d]Special Astrophysical Observatory, Nizhnyi Arkhyz, Karachaevo-Cherkessiy, 369169, Russia

(Received October 30, 2002)

A study of the structure of hot stars and the nature of their variability is presented. We propose a three-phase model for hot-star winds and calculate the X-ray line emission of the hot component of the wind in comparison with the XMM Newton X-ray spectrum of O4f star ζ Puppis. The results of high-resolution spectroscopy for some bright O stars are also presented. The line profile variability of bright O stars 19 Cep and λ Ori A is detected.

Keywords: Spectra of O–B stars; X-ray hot plasma

1 INTRODUCTION

There is diverse evidence of the existence of strong inhomogeneities of different kinds in the atmospheres of early-type stars (Fullerton et al., 1996; Lépine et al., 1996; Kaper et al., 1997; Eversberg et al., 1996; de Jong et al., 1999, 2001; Lépine and Moffat, 1999). These include the following: the random ejection of blobs or clumps into the stellar wind which are believed to be responsible for the random variability of line profiles and continuum in Wolf–Rayet stars; non-isotropic flows from rotating O–B stars, which result in the variable discrete absorption components (DACs) of such stars; rotationally modified flows from B–Be stars resulted in Saturn-like equatorial discs around them. As yet, the origins of these various types of structure remain unknown. We proposed a project 'Structure and variability of hot-star winds' aimed at improving our understanding of the evolution of massive stars, possessing powerful stellar winds on the base of modelling the modern astrophysical data at many wavelengths from infrared–optical to ultraviolet and X-ray. In this report we outline the preliminary results of our investigations.

* Corresponding author. E-mail: Alexander.Kholtygin@paloma.spbu.ru

ISSN 1055-6796 print; ISSN 1476-3540 online
DOI: 10.1080/1055679031000139424

2 X-RAY SPECTRA AND THE STRUCTURE OF HOT PLASMA IN THE WINDS

2.1 Three-Phase Model of Early-Type Star Winds

We propose a three-phase model of winds, supposing the winds to consist of two ensemble of dense clumps (hot clumps, $T = 10^6$–10^7 K; cold clumps, $T \approx 10^4$ K). The clumps are embedded in the warm $T \approx 10^5$ K interclump medium. This model develops the concept of the two-phase stochastic shock model (Oskinova et al., 2001b), assuming that numerous X-ray-emitting hot zones are produced by shocks in the stellar wind and embedded in the ambient medium. In the framework of the three-phase model we investigate the formation of X-ray spectra of hot stars in the region $\lambda = 1$–50 Å. Firstly we investigate the influence of small temperature fluctuations on the ionization state of the plasma and its X-ray spectra.

2.2 Differential Emission Measure of Plasma

The temperature and density distribution of hot gas in the wind can be described in terms of a double-differential emission measure (DEM) $\mu(T, N)$ (Judge et al., 1997). For generality we introduce the modified double-differential emission measure (MDEM)

$$\mu^*(T, N)\, dT\, dN = \mu(T, N)\, dT\, dN_e. \tag{1}$$

Here T is the local temperature of hot gas, N is its total local number density and N_e is the electron number density. We suppose that there is no differences between the electron and ion temperatures and hereafter use the electron temperature T_e instead of T.

2.2.1 Ionization State and Emitting Properties of the Plasma with Temperature and Density Fluctuations

The ionization state and emitting properties of the whole plasma is directly determined by its DEM or MDEM. The state of plasma in a selected volume depends on the differences $\delta T_e = |T_e - \bar{T}_e|$ and $\delta N_e = |N_e - \bar{N}_e|$, where $\bar{T}_e$ and $\bar{N}_e$ are the mean temperature and density respectively of the emitting plasma volume. In this section we consider a plasma with small temperature and density fluctuations: $\delta T_e \ll T_e$ and $\delta N_e \ll N_e$. For investigation of the impact of the T_e and N_e fluctuations on the global plasma parameters we use the generalization of the methods described by Peimbert (1967), Peimbert et al. (1995) and Kholtygin (1998, 2000). Let $\mathcal{Q}$ be any additive parameter, determined by the MDEM of the emitting volume:

$$\mathcal{Q} = \int\int q(T_e, N_e)\mu^*(T_e, N_e)\, dT_e\, dN_e, \tag{2}$$

where $q(T_e, N_e)$ is the distribution function of parameter $\mathcal{Q}$, and integration is fulfilled over all the volume V. Equation (2) is valid, for example, for the energy, emitted by a plasma in an arbitrary line, for the total plasma cooling function and for the total ionic abundances. Instead of T_e and n_e we use the dimensionless parameters $\theta = \log(T_e, K)$ and $\eta = \log(N_e\ cm^{-3})$. For

hot clumps in the atmospheres of the early-type stars, $\theta \approx 6$–7 and $\eta \approx 11$–13 (Waldron and Cassinelli, 2000). Next let us introduce parameters to describe the fluctuations in θ and η:

$$\begin{aligned} t^2 &= EM^{-1} \int\int\int_V (\theta - \bar{\theta})^2 n^2 \, dV, \; ts = EM \int\int\int_V (\theta - \bar{\theta})(\eta - \bar{\eta}) n^2 \, dV, \\ s^2 &= EM^{-1} \int\int\int_V (\theta - \bar{\theta})^2 n^2 \, dV, \end{aligned} \tag{3}$$

where EM is the total emission measure of the hot gas given by

$$EM = \int\int\int_V n^2 \, dV. \tag{4}$$

If the parameters t^2, ts and s^2 are small, then

$$\mathcal{Q} = \mathcal{Q}^0(1 + A_{tt}t^2 + A_{ts}ts + A_{ss}s^2), \tag{5}$$

where $\mathcal{Q}^0 = \mathcal{Q}(\bar{\theta}, \bar{\eta})$ is the value of $\mathcal{Q}$ at mean $t = \bar{t}$ and mean $s = \bar{s}$. The parameters A_{tt}, A_{ts} and A_{ss} are determined by the following expressions:

$$A_{tt} = \left[\frac{1}{2}\frac{\partial^2 q}{\partial t^2}\mathcal{Q}^{-1}\right]_{t=\bar{t};\, s=\bar{s}}, \quad A_{ts} = \left[\frac{\partial^2 q}{\partial t \, \partial s}\mathcal{Q}^{-1}\right]_{t=\bar{t};\, s=\bar{s}}, \quad A_{ss} = \left[\frac{1}{2}\frac{\partial^2 q}{\partial s^2}\mathcal{Q}^{-1}\right]_{t=\bar{t};\, s=\bar{s}}. \tag{6}$$

The parameters A_{tt} and A_{ss} describe the response of a value of the parameter $\mathcal{Q}$ on the small temperature and density fluctuations, while the parameters A_{ts} describe the temperature–density correlations. Our calculations show that at the values $n_e < 10^{13}$ cm^{-3} typical for solar and stellar coronae the parameters A_{ts} and A_{ss} are small (see also Kholtygin (1998) for a discussion); so only temperature fluctuations are important.

2.2.2 Ionization State of Plasma with Various Differential Emission Measure Distributions

Hereafter, we shall use the modified emission measure integrated over all electron number densities (the emission measure differential with respect to temperature, introduced by Craig and Brown (1976)):

$$\nu^*(T_e) \, dT_e = \int \mu^*(T_e, N_e) \, dN_e. \tag{7}$$

We shall use two simple models of MDEM distribution.

Model A (the log-normal distribution) is given by

$$\nu^*(T_e) \, d\theta = EM \frac{1}{\sigma(2\pi)^{1/2}} e^{-(1/2)[(\theta-\theta_0)/\sigma]^2} d\theta. \tag{8}$$

Model B (the two component model) is given by

$$\nu^*(T_e) \, d\theta = EM \, [q_1\delta(\theta - \theta_1) + q_2\delta(\theta - \theta_2)] \, d\theta, \tag{9}$$

where EM is the total emission measure of plasma, $q_1 = EM_1/EM$ and $q_2 = EM_2/EM$, where EM_1 and EM_2 are the emission measures for the $\theta_1 = \log(T_1)$ and $\theta_2 = \log(T_2)$ components.

For illustration the possible MDEM distributions for model A and different values of the parameter σ are presented in Figure 1(a).

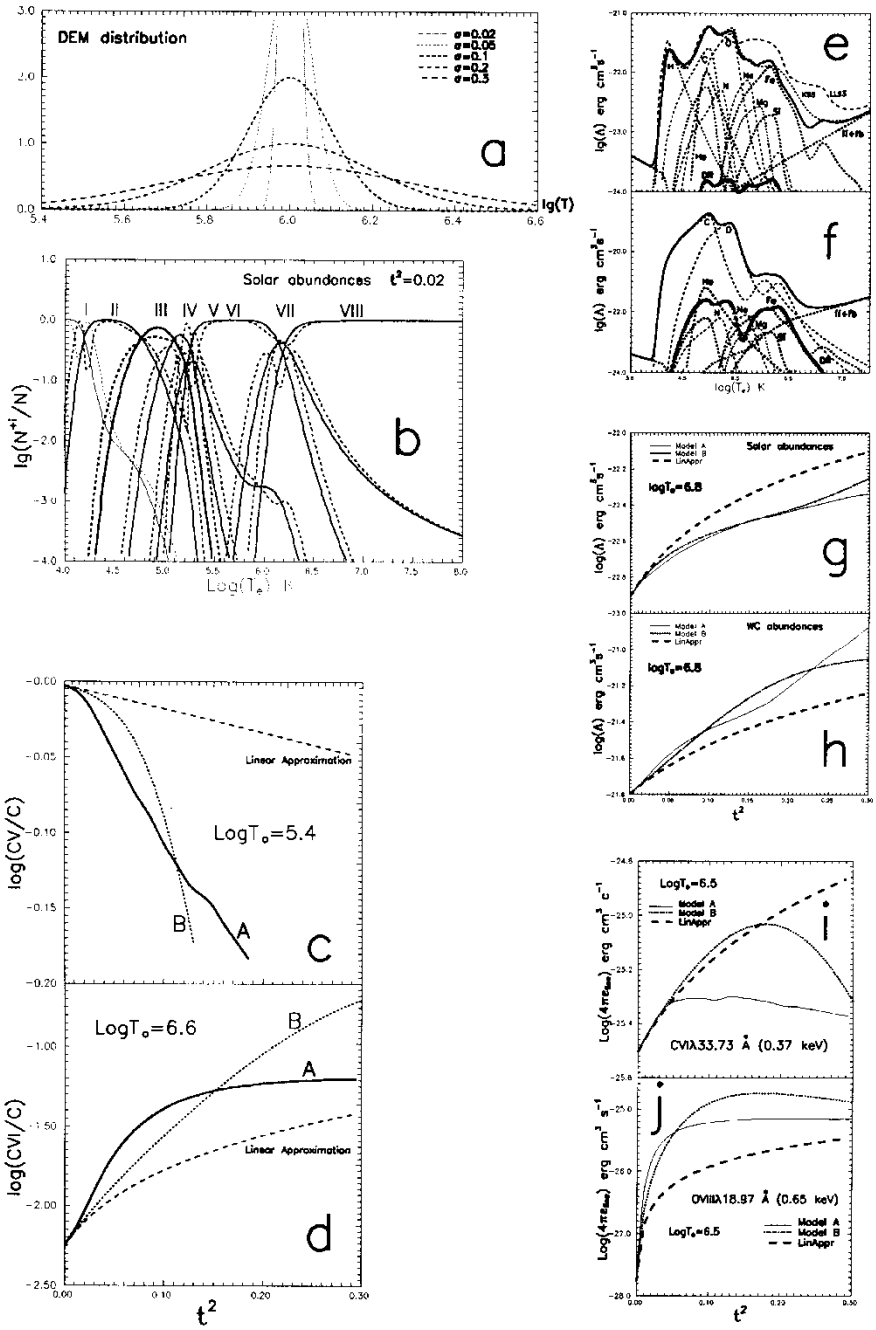

FIGURE 1 (a) Distribution of the DEM for various values of σ. (b) Relative N-ion abundances with (· · · · ·) and without (———) temperature fluctuations. (c), (d) Relative abundances of (c) the C V and (d) the C VI ions versus the parameter t^2. The letters on the curves denote the models for MDEM distributions. The linear approximation of small temperature fluctuations (· · · · ·) is also shown. (e) Cooling function for solar abundances and partial cooling contributions: curve DR, contribution of the dielectronic recombination; curve K93, cooling functions obtained by Kirienko (1993); curve LL99, cooling functions obtained by Landi and Landini (1999). (f) The same as in (e) but for standard WC abundances (see Table I). (g) Cooling function at log $T_e = 6.8$ for solar element abundances and for different models of DEM distribution. (h) The same as in (g), but for WC abundances. (i) Emission coefficient in the resonance line of the hydrogen-like ion C^{5+} for various models of DEM distributions in comparison with the calculated linear approximation. (j) The same as in (i), but for the ion O^{7+}.

The mean temperature $\bar{T}$ and the value of t^2 for plasma for models A and B are

$$\begin{aligned} &\bar{T}_e = e^{\theta_0},\ t^2 = \sigma^2 \quad \text{(model A)},\\ &\bar{T}_e = q_1 T_1 + q_2 T_2,\ t^2 = q_1 q_2 (T_2 - T_1)^2 \quad \text{(model B)}. \end{aligned} \tag{10}$$

The parameter t^2 in this relation is not mandatorily small.

For an illustration of the influence of the small temperature fluctuations on the ionization state of plasma we present the fractions of ions N^{i+} both for a homogeneous temperature medium and for a medium with a small fluctuations of $T_e(t^2 = 0.04)$ in Figure 1(b). For larger values of the parameter t^2 the linear approximation (10) cannot be valid as is shown in Figures 1(c) and (d) for the relative abundances of C ions.

2.3 Cooling Function

The cooling rate L for the plasma is determined as the energy emitted by a unit volume of plasma in unit time. In this paper we consider an optically thin plasma, the state of which is controlled by collisions of atoms and ions with electrons. A comparison of the X-ray spectra observed and calculated in the framework of the optically thin plasma models shows (Schulz et al., 2000) that this is a reasonable approximation. Moreover it should be mentioned that the existence of the velocity gradient between inside hot clumps themselves and between the different hot clumps in the wind leads to an effective decrease in the total line optical depth.

In this case, the local cooling rate is determined by the local electron temperature and density of the medium. We can express the cooling rate in term of the cooling function $\Lambda = L/n^2$. With partial ion abundances X_{ij} we can present a total cooling function as a sum over line and continuum:

$$\Lambda = \sum_{ij} X_{ij} \lambda_{ij} = \sum_{ij} X_{ij} (\lambda_{ij}^{\text{line}} + \lambda_{ij}^{\text{cont}}), \tag{11}$$

where $\lambda_{ij}^{\text{line}}$ and $\lambda_{ij}^{\text{cont}}$ are the partial cooling functions for lines and the continuum respectively. The calculated cooling functions for solar abundances and WC star abundances (hereafter called simply WC abundances) (van der Hucht et al., 1996) are plotted in Figures 1(e) and (f). The element abundances used are given in Table 1. As for WC stars the H abundances are negligible; we normalize the abundances to the solar abundance $\{Si\} = 7.55$.

TABLE I Element Abundances Used for the Cooling Function Calculation.

	$\{X\} = \log(N(X)/N(Si)) + 7.55$		
Element	Solar	WC	WC-to-solar
H	12.00	$-\infty$	0.0
He	10.99	11.79	6.3
C	8.55	11.40	708
N	7.97	7.97	1.0
O	8.87	11.11	174
Ne	8.08	8.08	1.0
Mg	7.58	7.58	1.0
Si	7.55	7.55	1.0
Fe	7.50	7.50	1.0

2.3.1 Cooling of Plasma with Various Double-Differential Emission Measure Distributions

We calculate the cooling function for models A and B of MDEM distribution. In Figure 1(g) and (h), we compare the cooling functions for different abundances and for various MDEMs. We can see that the linear approximation may not hold for $t^2 > 0.04$. It is important to note that models A and B with equal total emission measures and with identical mean electron temperatures but with different emission measure distributions produce quite different cooling functions.

2.4 X-ray Line Intensities for a Low-Density Plasma

2.4.1 Line Intensities for the Various Modified Double-Differential Emission Measures

We calculate the line emission coefficients for various MDEM distributions and for all X-ray lines included in the total cooling function calculation. The result of a comparison of the calculated emission coefficients with those obtained in the linear approximation is presented in Figures 1(i) and (j). We can see again that the linear approximation is not valid for $t^2 \geqslant 0.04$.

2.4.2 X-ray Line Intensities in the Spectra of Early-Type Stars

It has been proposed that the observed X-ray emission both in the lines and in the continuum is formed by the hot clumps in the wind. Both previous and recent (Waldron and Cassinelli, 2000; Kahn et al., 2001) X-ray observations show that an X-ray-emitting gas is distributed throughout the whole wind.

The applicability of the stationary approximation for hot clumps in the wind of early-type stars emitting in the X-ray region is not evident. It depends on the mean recombination times $\tau_{\rm rec}$, cooling time $\tau_{\rm cool}$ and dynamic time $\tau_{\rm dyn} = R/c$, where R is the mean size of the considered volume of plasma and c is the sound velocity. The recombination time $\tau_{\rm rec} = [N_e \alpha(T_e)]^{-1}$, where $\alpha(T_e)$ is the total recombination rate for the considered ion and cooling time $\tau_{\rm cool} = T/(dT/dt)$. If $\tau_{\rm rec} \ll \tau_{\rm cool}$ and $\tau_{\rm cool} \ll \tau_{\rm dyn}$, then we can use the stationary approximation.

The mean size of hot clumps in the wind is about $0.1R_\odot$. For typical hot-clumps $T \approx 10^7$ K (Aleksandrova and Bychkov, 2000), $\tau_{\rm din} \approx 1$ h.

In general, cooling of the hot plasma is determined by thermal conduction and radiation. For typical hot-clump conditions the thermal conduction cooling time is much longer than the radiative cooling time (see for example Cargill and Klimchuk (1997)) and we can consider the radiative cooling only. The radiative cooling time can be estimated from the evident relation $\tau_{\rm cool} \approx \frac{3}{2} kT/n\Lambda$. Using the value $n = 10^{11}$ cm^{-3} for outer layers of the hot star winds, we find $\tau_{\rm cool} \approx 1$. We have $\tau_{\rm rec} = 1$–10 s $\ll \tau_{\rm cool}$ and can conclude that hot clumps in the winds are in ionization equilibrium.

2.4.3 Emission Measure Distribution for O4Ief Star ζ Pup

Before modelling the X-ray spectra of the star, we have to select a realistic model for the MDEM distribution for the hot gas in the atmosphere. The best way is to use a model of hot-gas formation via its heating by the stochastic ensemble of the shock waves (Oskinova et al., 2001b). A good approximation for describing stochastic heating is the nanoflare concept proposed by Cargill (1994) and Klimchuk and Cargill (2001) to describe the heating of the solar coronal gas. In the framework of this concept the active region corona consists of

TABLE II X-ray Line Fluxes in the Spectra of O4Ief Star ζ Pup.

	F^{obs} (10^{-4} photons cm^{-2} S^{-1})		F^{calc} (10^{-4} photons cm^{-2} S^{-1})	
Si XIII (6.65, 6.69, 6.74)	1.10	0.32	0.78	1.05
Mg XII (8.42)	0.41	0.25	0.51	0.55
Mg XI (9.17, 9.23, 9.31)	2.00	0.39	1.13	1.01
Ne X (12.13)	1.80	0.93	2.31	2.66
Ne IX (13, 45, 13.55, 13.70)	5.00	0.98	2.37	2.76
Fe XVII (15.01, 15.26)	7.40	1.94	5.37	7.99
Fe XVII (16.78, 17.05, 17.10)	4.70	0.86	2.37	3.51
O VIII (18.97)	3.50	0.98	1.88	2.04
O VII (21.60, 21.80, 22.10)	5.10	3.63	5.14	7.21
N VII (24.78)	6.40	0.62	9.95	7.14
N VI (28.78, 29.08, 29.53)	11.30	0.50	4.25	5.04
C VI (33.74)	0.64	2.43	1.57	0.63
δF		5.82	0.76	0.42

many small randomly heated elemental loops. Model A gives a better fit than model B does to the MDEM calculated by Cargill (1994); so hereafter we shall use only this model.

Before fitting the observed and calculated line fluxes we have to consider the effect of the absorption of the X-ray photons in the surrounding cold wind. Recently, Ignace and Gayley (2002) found that the wind attenuation of the X-rays can significantly distort the X-ray line profiles, but the changes in the total line fluxes do not exceed 20%. The accuracy of the measured X-ray line fluxes is about this value or even lower (Kahn et al., 2001); so we do not correct the calculated line fluxes for wind attenuation.

The observed X-ray line fluxes are taken from the paper by Kahn et al. (2001). For the best fit we use three different sets of element abundances: the solar abundances given by Grevesse et al. (1996), the He, C, N and O abundances obtained by Hillier et al. (1993) from the analysis of the optical and X-ray spectra of ζ Pup and the fitted abundances obtained from conditions of the minimum of the rms deviation of the observed line flux F^{obs} and the calculated line flux F^{calc} (Table II).

The result of the line fit for different sets of element abundances are presented in Table 3. One can conclude that with the set of the solar element abundances we can obtain a fit of very poor quality; the quality of fit with the Hillier et al. (1993) abundances is much better. The optimal abundances obtained by us, which give the best fit to the observed line fluxes, are listed in the third column of Table IV. We can see from the table that N in the atmosphere of ζ Pup is highly abundant, whereas the carbon is underabundant as a result of enrichment of the matter of stellar wind by the products of the CNO cycle reactions.

In Table III the estimated optimal parameters of the MDEM distribution are given. In the third row of Table III we present the values of the total emission measures for X-ray-emitting matter. We accept the value of $d = 450$ pc (Schaerer et al., 1997) for the distance to the star. Using $EM = 6.5 \times 10^{60}$ cm^{-3} for the total emission measure of the smooth, spherically symmetric wind (Kahn et al., 2001) we can find the filling factor for X-ray-emitting matter: $\chi = EM_X/EM \approx 5 \times 10^{-6}$. This means that only a very small fraction of the wind matter emits in the X-ray region.

TABLE III Fits for Different Sets of Element Abundances.

	Solar abundance	Hillier et al. (1993)	Fitted abundance
$\log T_e^{opt}$	6.99	6.82	6.94
σ^{opt}	0.60	0.32	0.49
$\log EM_X^{total}$	55.4	55.6	55.5

TABLE IV Element Abundances for ζ Pup.

Element	{X} Hillier et al. (1993)	{X} Fitted	Fitted-to-Solar abundance ratio
H	12.00	12.00	1.0
He	11.08	11.08	1.0
C	8.23	7.88	0.2
N	8.92	8.92	8.9
O	8.82	9.06	1.5
Ne	8.08	8.38	2.0
Mg	7.58	7.79	1.6
Si	7.55	7.91	2.3
Fe	7.50	7.94	1.7

3 THE FAST VARIABILITY IN THE OPTICAL SPECTRA OF HOT STARS

3.1 Programme of Observations

The result of the hot clumps cooling in the wind of hot stars is the formation of a large number of dense cold clumps and can be responsible for the fast line profile variations in the optical spectra of the stars. To search for and analyse such rapid profile variability in spectra of these stars we propose a programme of spectral observations with a time resolution of 5–30 min or better. The list of programme stars is given in Table V. The list of stars observed in the 2001 campaign and the total number of spectra are presented in Table VI. In the present work we present the preliminary results for the stars λ Ori and 19 Cep.

3.2 Line Profile Variability

As a first step all spectra were normalized to the continuum level using the normalization procedure described by Shergin et al. (1996). Then we averaged all spectra obtained during the campaign for each of stars and subtracted the mean spectra from the individual spectra to obtain the difference spectra. An illustration of the mean spectrum of 19 Cep in selected orders is presented in Figure 2.

The profiles of many lines in the spectra of studied stars seem to be variable. For example, in Figures 3(a) and (b) the set of difference spectra of 19 Cep near the He I ($\lambda = 5876$ Å) and

TABLE V List of Programme Stars.

HD	Name	Spectrum type	V	V_∞^V [a]	$V_{rot} \sin i$ [a]
24212	ξ Per	O7.5III	4.04	2330	213
30614	α Cam	O9.5I	4.29	1590	129
36486	δ Ori	O9.5II	2.23	2060	144
36861	λ Ori A	O8III	3.66	2175	74
37742	ζ Ori A	O8III	1.79	1860	124
47839	15 Mon	O7Ve	4.66	2110	67
203064	68 Cyg	O8e	5.04	2340	115
209975	19 Cep	O9.5I	5.11	2010	95
210839	λ Cep	O6Iab	5.09	2300	219
214680	10 Lac	O9V	4.87	1140	35
91316	ρ Leo	B1Iab	3.84	1110	75

[a]From Kaper et al. (1997).

TABLE VI List of Stars Observed in 2001.

Observation dates	Object	Exposure (min)	Number of spectra	Total time observation (h)
September 4–7, 2001	ξ Per	10	4	0.7
	α Cam	10	11	1.8
	19 Cep	15	24	6.0
	10 Lac	10–15	39	10.5
November 29– December 7, 2001	ξ Per	5	5	0.4
	α Cam	10	6	1.0
	λ Ori A	10	75	12.5
	ζ Ori A	2	36	1.2
	10 Lac	15	27	6.7

C III ($\lambda = 5696$ Å) lines are given. One can see the variable details of the He I ($\lambda = 5876$ Å) line profile at an approximate velocity of $90\,\mathrm{km\,s^{-1}}$ from the line centre. Similar details are revealed in the profiles of Hα, Hβ and strong He lines in the spectra of the star. On the other hand, the C III ($\lambda = 5696$ Å) line in the spectra of the same star does not show the significant line profile variations (LPVs).

The variability of the line profiles can be more clearly manifested using the TVS analysis (Fullerton et al., 1996). The total TVSs for the He I and C III lines of 19 Cep are depicted in Figures 3(c) and (d) respectively. It is important to note that, if we smooth the difference spectra of investigated lines before the calculation TVS, the LPV is more evident. As we can see from Figures 3(e) and (f), such smoothing reveals the LPVs of the C IV ($\lambda = 5812$ Å) and C III ($\lambda = 5696$ Å) lines respectively; this cannot be seen in the difference spectra of these lines which were not smoothed.

Using the described techniques we reveal the variability of the Hα, He II ($\lambda = 4686$ Å) and C III ($\lambda = 5696$ Å) line profiles in the spectra of λ Ori that had not previously been known.

3.3 Wavelet Analysis of Line Profiles

An appropriate method to study the line profile variability is wavelet analysis (see for example, Lépine et al. (1996) and Kudryashova and Kholtygin (2001)). The integral wavelet transform can be written in the following form (see for example Dobeshi (1992)):

$$W(s, u) = \frac{1}{s}\int_{-\infty}^{\infty} f(x)\psi\left(\frac{x-u}{s}\right)\,dx. \tag{12}$$

Here $f(x)$ is the analysed signal and we choose the so-called Mexican Hat (MHAT) wavelet $\psi(x) = (1 - x^2)e^{-x^2/2}$, as the analysing (mother) wavelet $\psi(x)$. It has a narrow energy spectrum and zero-valued zeroth and first moments.

The signal energy density $E_W(s, u) = W^2(s, u)$ describes the distribution of the analysed signal in (s, u) = (scale, coordinate) space. For the line profiles the coordinate x is the wavelength; so the scale variable s can be expressed in ångströms.

The total energy of the signal over the scales is distributed in accordance with the wavelet power spectrum (WPS)

$$E_W(s) = \int_{u_1}^{u_2} W^2(s, u)\,du = \int_{u_1}^{u_2} E_W(s, u)\,du. \tag{13}$$

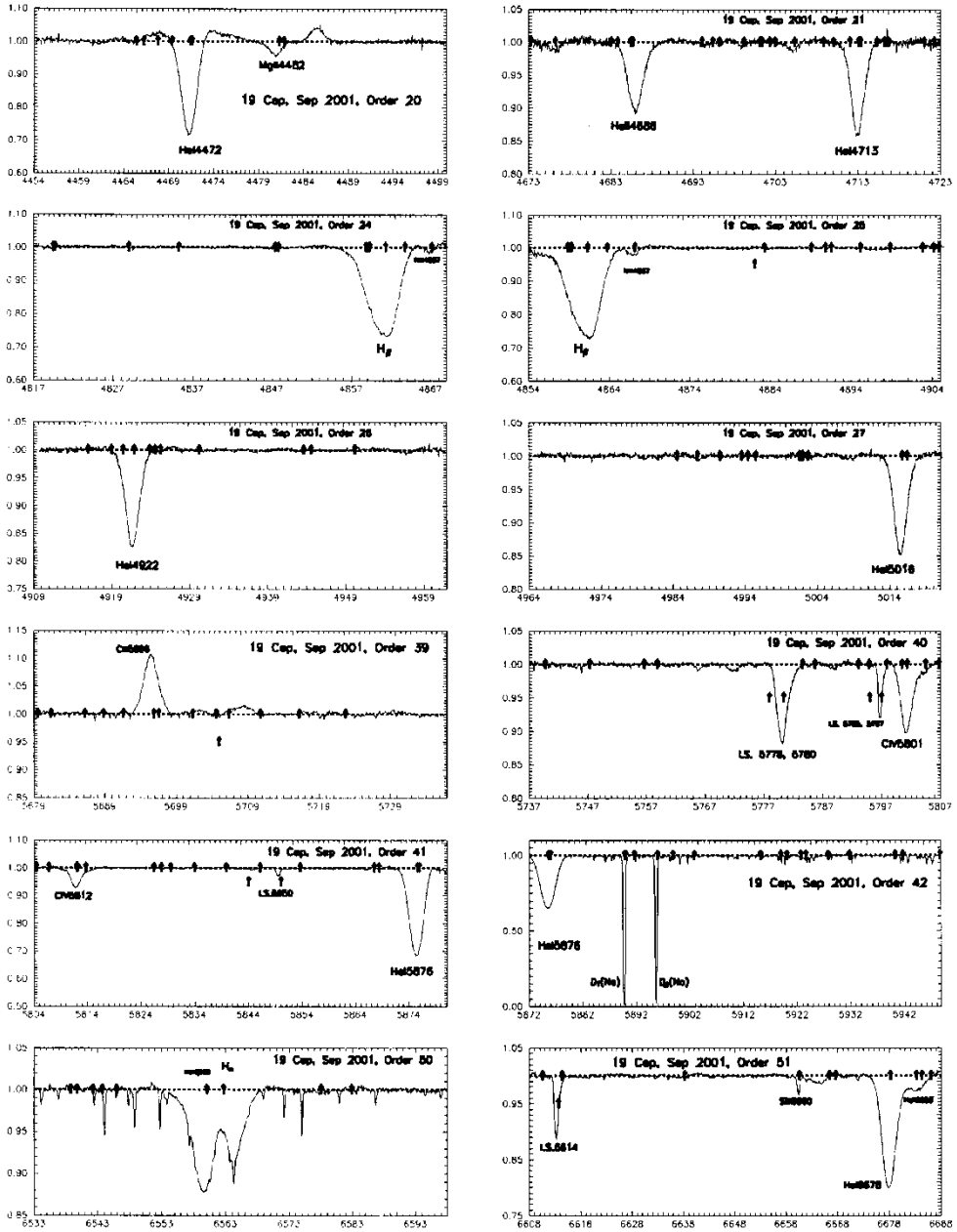

FIGURE 2 The mean spectra of the star 19 Cep. Thick arrows indicate the laboratory wavelengths of contributed lines in the spectra.

The obtained WPSs for the C III ($\lambda = 5696$ Å) line in a spectrum of λ Ori are presented in Figure 4(a). From the figure we can see the presence of the small-scale (0.1–1.0 Å) and the large-scale (1.0–8 Å) components in the WPSs.

The first component includes the noise contribution with a maximum near the pixel size of about 0.07 Å. In this component we can also see the contribution of additional variable small-scale component at 0.2–0.6 Å (10–30 km s^{-1}). This is possibly connected with the

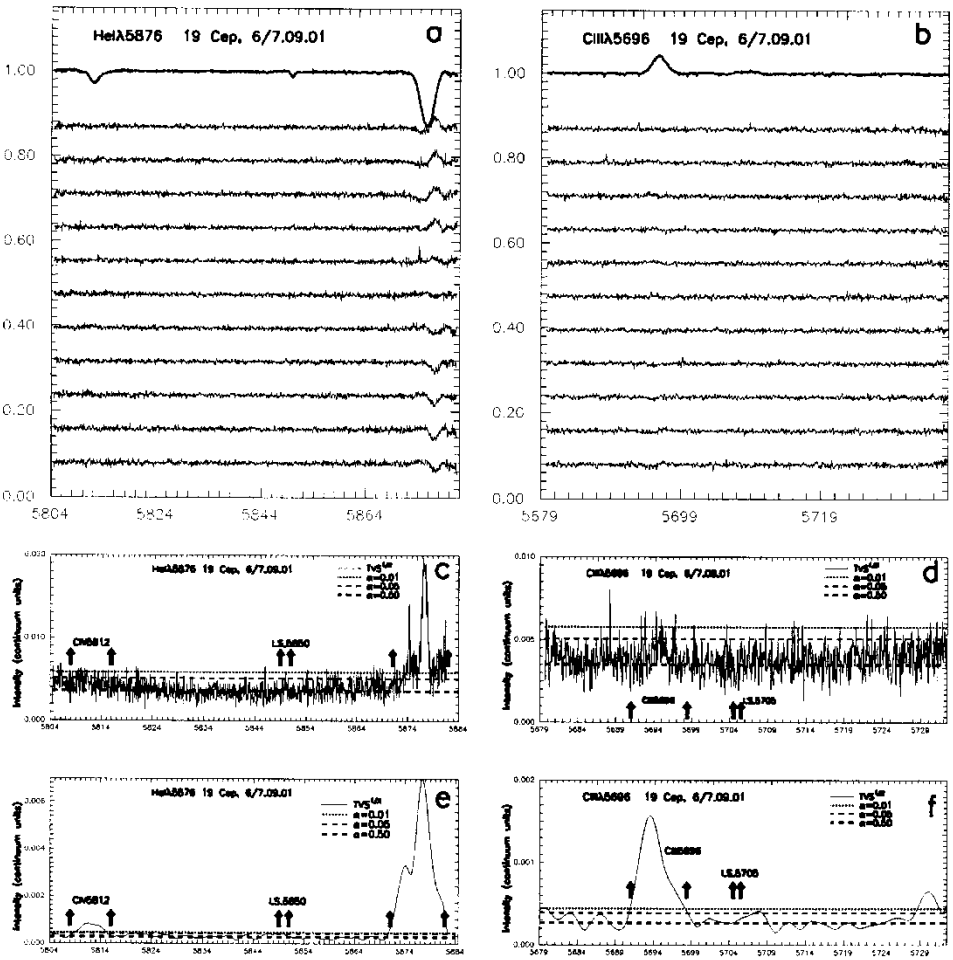

FIGURE 3 The line profile variations in the spectra of studied stars. (a) Temporal variances in the difference profile of the He I ($\lambda = 5876$ Å) line in the spectrum of the star 19 Cep. (b) The same as in (a), but for the C III ($\lambda = 5696$ Å) line. (c) The time variation spectrum (TVS) for the He I ($\lambda = 5876$ Å) line: – – –p = 0.01; $\cdots$, p = 0.5. (d) The same as in (c), but for the C III ($\lambda = 5696$ Å) line. (e) The same as in (c), but after smoothing with a Gaussian filter ($\sigma = 2$ Å). (f) The same as in (e), but for the C III ($\lambda = 5696$ Å) line.

small clumps in the winds of the star. The second component is strongly variable (the dominant scale is 2–4 Å or 100–200 km s^{-1}) and is connected with large-scale structures in the winds.

3.3.1 Searching the Periodic Variations

To investigate the temporary variations in the WPS we choose the wavelength interval $[S_1, S_2] = 3.0$–4.0 Å, where variations in the WPS are maximal (see Figure 4(a)). The integrated WPS in the selected interval is

$$E_{[S_1,S_2]}(t) = \int_{S_1}^{S_2} E_W(s, t)\, ds, \tag{14}$$

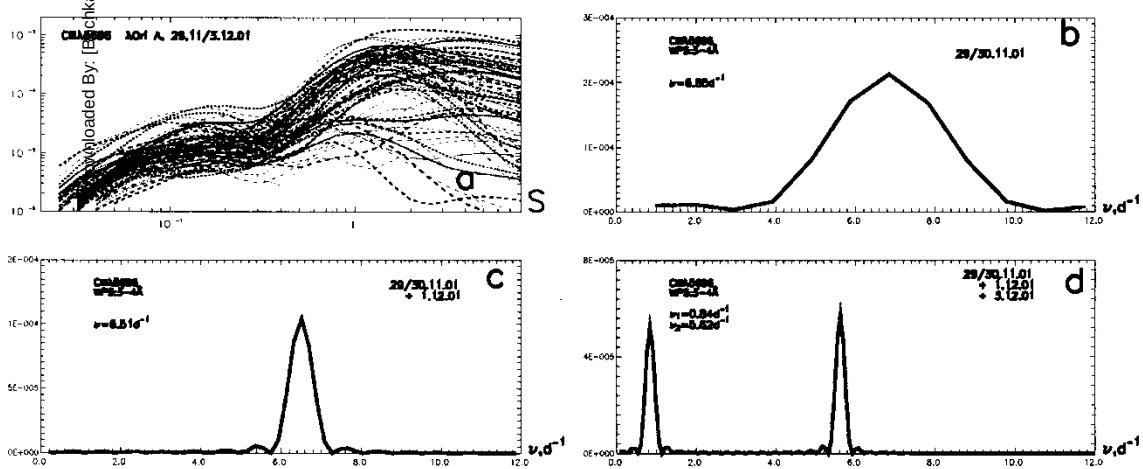

FIGURE 4 (a) WPSs for the C III ($\lambda = 5696$ Å) line in the spectra of λ Ori A. (b) the CLEANed Fourier spectrum integrated in the region 3.0–4.0 Å on observations made on November 29–30, 2001 (28 spectra). (c) The same as in (b), but for November 29–30, 2001, and December 1, 2001 (52 spectra). (d) The same as in (b), but for November 29–30, 2001, December 1, 2001, and December 3, 2001 (75 spectra). The frequencies of the detected Fourier components are given.

where $E_W(s, t)$ is the WPS for the line profile observed at the moment t. Fourier analysis based on the iterative CLEAN algorithm (Roberts et al., 1987) was used to search for periodic variability.

The CLEANed Fourier spectra of the function $E_{[S_1, S_2]}(t)$ for the C III ($\lambda = 5696$ Å) line in the spectrum of λ Ori A are given in Figures 4(b)–(d). We can see the enhancement of the frequency resolution including the new observations in the calculation of the Fourier spectrum. The smaller detected frequency $\nu_1 = 0.84$ days^{-1} gives the period of time variation as $P = 1.2$ days. Such periods was founded for variations in the profile of the Hα line in the spectra of selected O stars and are usually connected with the rotational modulation of line profiles (Kaper et al., 1997). This result is the first detection of a long-time-scale regular variability for an emission line in the spectra of O stars. We plan to obtain a longer time series for this line to confirm this detection.

In the light of our hypothesis on the connection between the hot clumps, which form X-ray emission, and the cold clumps, which are responsible for the LPVs of optical lines, the long-time-scale variability of optical lines has to be reflected in the variability of the X-ray lines and continuum fluxes of O stars. Recently Oskinova et al. (2001a) reported the rotational modulation of the X-ray emission from the O star ζ Oph, observed by ASCA X-ray satellite (0.5–10 keV) with a period $P \approx 0.77$ days close to the recurrence time (0.875 ± 0.167 days) of the DACs. This supports the proposed hypothesis and is a good start point for searching the connection between the X-ray and the optical variabilities for other O stars.

The larger frequency $\nu_1 = 5.62$ days^{-1} found corresponds to the period $P = 4.3$ h and is typical for non-radial pulsations (NRPs) of O stars (de Jong et al., 1999). The effect of NRPs was never detected in profiles of emission lines; so the nature of this short-time-scale variability is not evident and future detailed investigations are necessary.

Acknowledgements

The authors are grateful for the support provided by the NATO collaborative linkage Grant CLG 6978036 and RFBR Grant 01-02-16858.

References

Aleksandrova, A. and Bychkov, K. V. (2000). Astron. Rep., 44, 781.
Cargill, P. J. (1994). Astrophys. J., 422, 381.
Cargill, P. J. and Klimchuk, J. A. (1997). Astroph. J., 478, 799.
Craig, I. J. D. and Brown, J. C. (1976). Astron. Astrophys., 49, 239.
de Jong, J. A., Henrichs, H. F., Kaper, L., Nichols, J. S., Bjorkman, K., et al. (2001). Astron. Astrophys., 368, 601.
de Jong, J. A., Henrichs, H. F., Schrijvers, S., Gies, D. R., Telting, J. H., Kaper, L. and Zwarthoed, G. A. A. (1999). Astron. Astrophys., 345, 172.
Dobeshi, I. (1992). Ten Lectures on Wavelets. Philadelphia, Pennsylvania.
Eversberg, T., Lépine, S. and Moffat, A. F. J. (1998). Astrophys. J., 494, 799.
Fullerton, A. W., Gies, D. R. and Bolton, C. T. (1996). Astrophys. J., Suppl. Ser., 103, 475.
Grevesse, N., Noels, A. and Sauval, A. J. (1996). ASP Conf. Series, Vol. 99. Proc. 6th annual Astroph. Conf. in College Park, Maryland, 9–11th October 1995; San Francisco, ed. by Stephen S. Holt and George Sonneburn, p. 117.
Hillier, D. J., Kudritzski, R., Pauldrach, A. W. A., Baade, D., Cassinelli, J. P., Puls, J. and Schmitt, J. H. M. M. (1993). Astron. Astroph., 276, 117.
Ignace, R. and Gayley, K. G. (2002). Astrophys. J., 568, 954.
Judge, P. G., Hubeny, V. and Brown, J. C. (1997). Astrophys. J., Suppl. Ser., 475, 275.
Kahn, S. M., et al. (2001). Astron. Astrophys., 365, 365.
Kaper, L., Henrichs, H. F., Fullerton, A. W., Ando, H., et al. (1997). Astron. Astrophys., 327, 281.
Kaper, L., Henrichs, H. F., Nichols, J. S. and Telting, J. H. (1999). Astron. Astrophys., 344, 231.
Kholtygin, A. F. (1998). Astron. Astrophys., 329, 691.
Kholtygin, A. F. (2000). Astrophysics, 43, 463.
Kirienko, A. (1993). Astron. Lett., 19, 11.

Klimchuk, J. A. and Cargill, P. J. (2001). Astrophys. J., 553, 440.
Kudryashoya, N. A. and Kholtygin, A. F. (2001). Astron. Rep., 45, 287.
Landhi, E. and Landini, M. (1999). Astron. Astrophys., 347, 401.
Lépine, S. and Moffat, A. F. J. (1999). Astrophys. J., 514, 909.
Lépine, S., Moffat, A. F. J. and Henriksen, R. N. (1996). Astrophys. J., 466, 392.
Oskinova, L. M., Clarke, D. and Pollock, A. M. T. (2001a). Astron. Astrophys., 378, L21.
Oskinova, L. M., Ignace, R., Brown, J. C. and Cassinelli, J. P. (2001b). Astron. Astrophys., 373, 1009.
Peimbert, M. (1967). Astrophys. J., 150, 825.
Peimbert, M., Torres-Peimbert, S. and Luridiana, V. (1995). Rev. Mex. Astron. Astrofís., 31, 131.
Roberts, D. H., Leh, J. and Dreher, J. W. (1997). Astron. J., 93, 968.
Schaerer, D., Schmutz, W. and Grenon, M. (1997). Astrophys. J., 484, L153.
Schulz, N. S., Canizares, C. P., Huenemoerder, D. and Lee, J. C. Astrophys. J., 545, L135.
Shergin, V. S., Kniazev, A. Yu. and Lipovetsky, V. A. (1996). Astron. Nachr., 317, 952.
van der Hucht, K. A., Cassinelli, J. P. and Williams, P. M. (1996). Astron. Astrophys., 168, 111.
Waldron, W. L. and Cassinelli, J. P. (2000). Astrophys. J., 548, L45.